

## Earth-Based Observations of the Galileo Probe Entry Site

G. Orton, J. L. Ortiz, K. Baines, G. Bjoraker, U. Carsenty, F. Colas, A. Dayal, D. Deming, P. Drossart, E. Frappa, J. Friedson, J. Goguen, W. Golisch, D. Griep, C. Hernandez, W. Hoffmann, D. Jennings, C. Kaminski, J. Kuhn, P. Laques, S. Limaye, H. Lin, J. Lecacheux, T. Martin, G. McCabe, T. Momary, D. Parker, R. Puetter, M. Ressler, G. Reyes, P. Sada, J. Spencer, J. Spitale, S. Stewart, J. Varsik, J. Warell, W. Wild, P. Yanamandra-Fisher, G. Fazio, J. Hora, L. Deutsch

Earth-based observations of Jupiter indicate that the Galileo probe probably entered Jupiter's atmosphere just inside a region that has less cloud cover and drier conditions than more than 99 percent of the rest of the planet. The visual appearance of the clouds at the site was generally dark at longer wavelengths. The tropospheric and stratospheric temperature fields have a strong longitudinal wave structure that is expected to manifest itself in the vertical temperature profile.

Remote sensing observations of the Galileo probe entry site (PES) near the time of entry were necessary to determine the characteristics of the site as compared with those of the rest of the heterogeneous and dynamic jovian atmosphere. Probe results may also serve as a measure of ground truth for remote sensing observations. The decision to use the spacecraft memory as the primary storage of probe data precluded the orbiter from acquiring remote sensing measurements of the PES, which meant that only Earth-based observations (1) (Table 1) could fulfill this role.

Most of the observations were of sunlight scattered from Jupiter's clouds at wavelengths  $<5\ \mu\text{m}$  (Fig. 1). The Galileo probe entered near the southern edge but inside an area that is dark at red wavelengths, although possibly not as dark as the center of the feature. At shorter wavelengths, the feature is brighter, giving it a dark blue-gray appearance. The one exception to this dark appearance at longer wavelengths is at  $1.58\ \mu\text{m}$ , a wavelength of minimal gaseous absorption that should be sensitive only to cloud particle albedo, whose more complicated appearance (Fig. 1D) was verified in several individual images used in the average. Images of the cloud field taken by the Hubble Space Telescope (HST) on 5 October 1995 show that at  $0.953\ \mu\text{m}$  (Fig. 2A), this feature was neither as large nor as dark as

on 7 December. Discrete spectral measurements of the reflectivity of the PES and a lighter region immediately to its south, taken within a few days of the probe entry, show that contrast between these regions is greatest ( $\sim 30\%$ ) between  $0.5$  and  $1.0\ \mu\text{m}$ . This is also true of the feature centered some  $22^\circ$  to the east in the 5 October HST images, which is close in appearance to the dark feature at the PES on 7 December.

Observations were also made at  $4.85\ \mu\text{m}$ , where Jupiter's spectrum is minimally affected by gaseous absorption and the outgoing radiance is dominated by thermal emission rather than reflected sunlight (Fig. 2, B through E). The brightest (hottest) regions signify thermal emission from the warmer depths of the atmosphere that are least obscured by atmospheric particulates. The bright regions (Fig. 2B) correlate with the positions of dark regions in the  $953\text{-nm}$  HST map (Fig. 2A) taken  $\sim 10$  hours afterward. These  $5\text{-}\mu\text{m}$  hot spots (2) typically cover less than 1% of the area of the planet and  $\sim 15\%$  of the PES latitude. They typically show  $4.85\text{-}\mu\text{m}$  radiances equivalent to a 255-K blackbody for near-nadir views and a 240-K blackbody for a hemispherical average. We note that the highly attenuated 7 December map is completely consistent with time-interpolated versions of the 21 November 1995 and 21 January 1996 maps when blurred further by atmospheric seeing. Therefore, it appears likely that the probe entered just within the thermally warm and visually dark area associated with the  $5\text{-}\mu\text{m}$  hot spot.

Determinations of stratospheric temperatures near the 0.01-bar level and of tropospheric temperatures near the 0.25-bar level were made from Infrared Telescope Facility (IRTF) observations of  $\text{CH}_4$  emission near  $7.8\ \mu\text{m}$  and  $\text{H}_2$  emission near  $18\ \mu\text{m}$ , respectively, by techniques used in earlier work (3, 4). The PES was located along meridional

G. Orton, J. Friedson, T. Martin, P. Yanamandra-Fisher, Mail Stop 169-237, Jet Propulsion Laboratory (JPL), California Institute of Technology, Pasadena, CA 91109; J. L. Ortiz, Mail Stop 169-237, JPL, and Instituto de Astrofísica de Andalucía, CSIC, P.O. Box 3004, 18080 Granada, Spain; K. Baines, Mail Stop 183-601, JPL; G. Bjoraker, D. Deming, D. Jennings, G. McCabe, P. Sada, Code 693, NASA Goddard Space Flight Center, Greenbelt, MD 20771; U. Carsenty, DLR Institute for Planetary Exploration, Rudower Chaussee 5, D-12489 Berlin, Germany; F. Colas, Bureau des Longitudes, 75015 Paris, France; A. Dayal and W. Hoffmann, Stewart Observatory, Univ. of Arizona, Tucson, AZ 85721; P. Drossart and J. Lecacheux, DESPA, Observatoire de Paris-Meudon, 92195 Meudon Cedex, France; E. Frappa and P. Laques, Observatoire Midi-Pyrenees, 65200 Bagneres de Bigorre, France; J. Goguen, Mail Stop 183-501, JPL; W. Golisch, D. Griep, C. Kaminski, J. Hora, Institute for Astronomy, Univ. of Hawaii, Honolulu, HI 96822; C. Hernandez, 9430 S.W. 29 Terrace, Miami, FL 33165; J. Kuhn, H. Lin, J. Varsik, National Solar Observatory, Sunspot, NM 88349; S. Limaye, Space Science and Engineering Center, Univ. of Wisconsin, Madison, WI 53706; T. Momary, 3806 Geology Building, Univ. of California, Los Angeles, CA 90024-1567; D. Parker, 12911 Lerida Street, Coral Gables, FL 33156; R. Puetter, CASS, Univ. of California at San Diego, La Jolla, CA 92093-0111; M. Ressler, Mail Stop 169-506, JPL; G. Reyes, Mail Stop 300-329, JPL; J. Spencer, Lowell Observatory, 1400 Mars Hill Road, Flagstaff, AZ 86001; J. Spitale and S. Stewart, Division of Geological and Planetary Sciences, 170-20, California Institute of Technology, Pasadena, CA 91125; J. Warell, Uppsala Astronomical Observatory, Box 515, S-75120 Uppsala, Sweden; W. Wild, Department of Astronomy and Astrophysics, Univ. of Chicago, Chicago, IL 60637; G. Fazio, Smithsonian Astrophysical Observatory, Cambridge, MA 02138; L. Deutsch, Five College Astronomy Department, Univ. of Massachusetts, Amherst, MA 01003.

**Table 1.** Galileo probe support observations of Jupiter in late 1995 to early 1996. Broadband filters had the following approximate wavelengths: B, 400 to 500 nm; V, 500 to 600 nm; R, 600 to 700 nm; I, 750 to 900 nm; Z, 850 to 950 nm; J, 1.1 to 1.4  $\mu\text{m}$ ; H, 1.5 to 1.8  $\mu\text{m}$ ; and K, 1.9 to 2.5  $\mu\text{m}$ . The other filters have bandwidths  $<5\%$  of the central wavelength listed. WFPC2, Wide Field Planetary Camera; CCD, charge-coupled device; res., resolution; and Obs., observatory.

Site and dates of observations	Instrument and comments
Hubble Space Telescope (5 and 7 Oct.)	WFPC2 (255- to 953-nm, high-res. CCD camera)
McMath-Pierce Solar Telescope, Kitt Peak* (4–11 Dec.)	CELESTE [high-res. spectrometer (12.2 and 13.6 $\mu\text{m}$ )] LEISA (1- to 2.5- $\mu\text{m}$ camera) CCD (618 and 656 nm) and video camera
NASA Infrared Telescope Facility* (2–10 Dec.)	NSFCAM (1- to 5- $\mu\text{m}$ camera) MIRAC2 (2- to 21- $\mu\text{m}$ camera) MIRLIN (5- to 24- $\mu\text{m}$ camera)
Pic-du-Midi Obs.* (6 Nov.–5 Dec.)	CCD (I)
Donald C. Parker Obs.* (4 and 7 Dec.)	CCD (B, V, R)
Swedish Solar Obs.* (22 Nov.–8 Dec.)	CCD (B, V, R, I, Z; 750, 829, 893, and 945 nm)
Vacuum Tower Telescope, Sacramento Peak (8 Dec.)	Near-infrared camera (J, H, and K)
Yerkes Obs.* (24 Nov. and 7 Dec.)	CCD (618, 727, and 945 nm)

\*Longer term Galileo support programs have been and are running at these facilities, with a particularly intensive program at the NASA IRTF.

tropospheric and stratospheric temperature gradients of 0.17 and 0.10 K per degree of latitude, respectively, consistent with Voyager data (5). Zonal waves in the stratospheric and tropospheric temperature fields extend several degrees north and south of the PES latitude, with amplitudes of 1 to 3 K at the PES latitude. In September through December maps of the temperature field, the stratospheric wave structure appears virtually fixed in position relative to System III, and the tropospheric wave structure appears to be moving at  $-2 \text{ m s}^{-1}$  (6). Both are moving much slower than the cloud field. Another type of wave structure is also present in the stratospheric temperature field. After May 1995, while zonal mean tropospheric temperatures remained roughly constant, zonal mean stratospheric temperatures at the PES latitude dropped by some 1 to 2 K, similar to a 1985 to 1986 global equatorial cooling [figure 3 of (4)]. Finally, our high-resolution spectroscopic observations of  $\text{C}_2\text{H}_6$  (ethane) stratospheric emission at  $12.16 \mu\text{m}$  at the PES are consistent with a volume mixing ratio of  $\sim 1 \times 10^{-6}$  near the 0.005-bar pressure level, assuming the stratospheric structure given in (7).

Earlier quantitative studies of reflected sunlight (8) and thermal emission (9) from

$5\text{-}\mu\text{m}$  hot spots suggest that they (i) have the lowest density of cloud particles  $\geq 1 \mu\text{m}$  in diameter and (ii) represent a region of relatively dry, downwelling gas. The relatively unusual nature of the entry site could explain the relative absence of particulates detected by the probe nephelometer (10) and net flux radiometer (11) experiments relative to preentry expectations. Two different analyses of spectroscopic data on  $5\text{-}\mu\text{m}$  hot spots (9) reached quite different conclusions about the abundance of water and properties of a water condensate cloud; together they bounded the directly sensed results (10–12). The waves sensed in the temperature field are not always present (13); they are phenomena (14) that should also appear as waves in the vertical temperature profile in the upper troposphere and lower stratosphere in a more detailed reduction of the data from the atmospheric structure experiment (7).

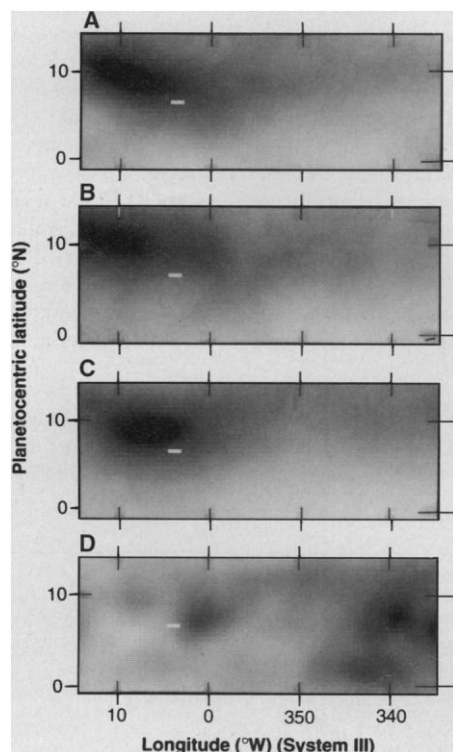


**Fig. 1.** Maps of cloud reflectivity at the PES from (A) Donald C. Parker Observatory on 7 December 1995 ( $0.61 \mu\text{m}$ ), (B) the Swedish Solar Telescope on 3 December ( $0.66 \mu\text{m}$ ), (C) Pic du Midi on 5 December ( $0.84 \mu\text{m}$ ), and (D) the IRTF on 21 November ( $1.58 \mu\text{m}$ ) (19). The location of the probe during descent, from 350 km above the 1-bar level to the 1-bar level and deeper, is given by the positions of the left and right sides of the short line, respectively.

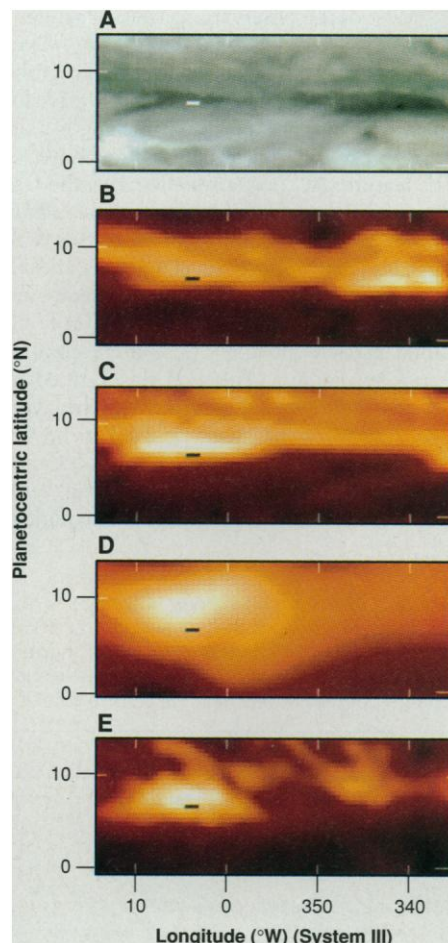


**Fig. 2.** Maps near the PES of (A) cloud reflectivity ( $0.953 \mu\text{m}$ ) from HST observations on 5 October 1995 and (B through E) thermal emission ( $4.85 \mu\text{m}$ ) (denoted by the false reddish color) from IRTF observations on (B) 5 October 1995, (C) 21 November, (D) 7 December, and (E) 22 January 1996 (19). The poorer resolution of the 7 December map arises from the large attenuation by the polypropylene safety screen.

## REFERENCES AND NOTES

- Observations from Earth close to the arrival date were challenging because Jupiter was only  $9^\circ$  from the center of the sun. Extensive baffling of the optical beam was used at several telescopes to reject sunlight and stabilize the image. At IRTF, a thin sheet of polypropylene was laid over the primary mirror, allowing transmission of only infrared radiation.
- These regions were first detected by J. Westphal [*Astrophys. J.* **157**, 63 (1969)] and described in detail by J. Westphal, K. Matthews, and R. Terile [*ibid.* **188**, 111 (1974)].
- G. S. Orton *et al.*, *Science* **252**, 537 (1991).
- G. S. Orton *et al.*, *ibid.* **265**, 625 (1994).
- Our  $7.8\text{-}\mu\text{m}$  IRTF images in December were strongly degraded by the attenuation of the polypropylene safety screen (1), and our derived stratospheric temperatures are noisy, with little recognizable zonal structure. Our initial conclusions about stratospheric temperatures at the PES are based on a longitudinal average (zonal mean), and tentative conclusions about motions of waves are based on correlation with the brightest zonal feature at the PES latitude.
- P. J. Gierasch, B. J. Conrath, J. A. Magalhaes, *Icarus* **67**, 456 (1986). We note, however, that the zonal mean stratospheric temperature variations displayed an unusually high correlation with those in the troposphere.
- A. Seiff *et al.*, *Science* **272**, 846 (1996).
- As summarized by R. West, D. Strobel, and M. Tomasko [*Icarus* **65**, 161 (1986)].
- B. E. Carlson, A. A. Lacis, W. B. Rossow, *J. Geophys. Res.* **98**, 5251 (1993); G. L. Bjoraker, H. P. Larson, V. G. Kunde, *Astrophys. J.* **311**, 1058 (1986).
- B. Ragent, D. S. Colburn, P. Avrin, K. A. Rages, *Science* **272**, 856 (1996).
- L. Sromovsky *et al.*, *ibid.*, p. 853.
- H. Niemann *et al.*, *ibid.*, p. 848.
- The waves were not apparent during, for example, the intensive observing by IRTF associated with the collision of Shoemaker-Levy 9 [G. Orton *et al.*, *Science* **267**, 1277 (1995)].
- One such phenomenon is the quasi-quadrennial oscillation [C. B. Leovy, A. J. Friedson, G. S. Orton, *Nature* **354**, 380 (1991)].
- S. Limaye, *Icarus* **65**, 335 (1986); and references therein.
- R. F. Beebe, A. A. Simon, L. F. Huber, *Science* **272**, 842 (1996).
- D. H. Atkinson, J. B. Pollack, A. Seiff, *ibid.*, p. 843.
- Pic-du-Midi images were processed to remove low-frequency signal variations; the other images underwent goodness-of-fit and PIXON restoration techniques [R. C. Puetter *Int. J. Imaging Syst. Technol.* **6**, 314 (1995); and references therein].
- Longitudes in both figures have been corrected for the motion of large-scale cloud features, measured during the preceding months at  $103.0 \pm 0.5 \text{ m s}^{-1}$  relative to the rotation of the interior (System III). This value is consistent with Voyager (15) and HST (16) results, although the PES itself was characterized by a much stronger prograde jet over a narrower region (16, 17). Image restoration processing (18) was applied before mapping, and corrections were made for illumination and emission angle variations across the map. The uncertainty of the PES position in these maps [Fig. 1:  $\sim \pm 2^\circ$  in latitude and longitude for (A),  $\pm 1^\circ$  for (B) and (C), and  $\leq 0.5^\circ$  for (D); Fig. 2:  $\ll 1^\circ$  for (A),  $\leq \sim 0.5^\circ$  for (B) and (C), and  $\sim 1^\circ$  to  $2^\circ$  for (D)] arises from uncertainty in fitting the limb.
- We thank the staff of several observatories for their support in making a number of unusual but important changes to observing techniques and schedules. The mapping in Fig. 2A was kindly provided by A. Simon and R. Beebe. Our research was sponsored by various grants from NASA and NSF for work performed at each of the institutions with which we are associated. K.B., A.D., J.F., J.G., W.H., T.M., J.L.O., G.O., M.R., G.R., J. Spencer, J. Spitale, S.S., and P.Y.-F. were visiting astronomers at IRTF, which is operated by the University of Hawaii under contract to NASA. We also thank the French Programme National de Planetologie for support of the Pic-du-Midi observations. P.S. was supported by a NASA–National Research Council Resident Research Associateship.

1 March 1996; accepted 16 April 1996